In Vivo Imaging Reveals an Essential Role for Neutrophils in Leishmaniasis Transmitted by Sand Flies

Nathan C. Peters, *et al.*

Science **321**, 970 (2008);
DOI: 10.1126/science.1159194

Science (print ISSN 0036-8075; online ISSN 1095-9203) is published weekly, except the last week in December, by the American Association for the Advancement of Science, 1200 New York Avenue NW, Washington, DC 20005.

laboratory as was done with strain PHS-1 (Fig. 3, A and B). Nevertheless, pure cultures of certain cyanobacteria (e.g., *Oscillatoria limnetica*) are known to use sulfide as an electron donor in anoxygenic photosynthesis (*19*). The oxidation of As(III) to As(V) by the Paoha cyanobacteria may be a second example of a two-electron transition—being analogous to the oxidation of H_2S to S^0 by *O. limnetica* (*19*). Phototrophic microorganisms may also contribute to As(III) oxidation in other environments, such as the chemically diverse hot springs of Yellowstone National Park, many of which contain arsenite (*20*–*22*), thereby broadening the ecological importance of the phenomenon described here.

Despite the clear evidence for arsenite oxidation by strain PHS-1, we were unable to obtain an amplicon for arsenite oxidase (*aoxB*) (*17*). This result was surprising because the gene is highly conserved across broad phylogenetic lineages (*23*) and primer sets have been successfully used for identifying *aoxB* in both pure cultures and environmental samples (*22*, *24*). An amplicon was obtained when primers for dissimilatory arsenate reductase designed for halophilic prokaryotes (*25*) were used. This occurred even though strain PHS-1 did not grow in the dark with 10 mM As(V) as the electron acceptor and 10 mM lactate, 10 mM acetate, or 4 mM sulfide as the electron donor [i.e., no loss of As(V) or production of As(III) and all optical densities (ODs) remained below 0.07 after 8 days of incubation]. The putative ArrA homolog for strain PHS-1 showed a high degree of sequence identity (~68%) to proteins from two other *Ectothiorhodospiraceae*, *Alkalilimnicola ehrlichii* and *Halorhodospira halophila* (Fig. 3D). *A. ehrlichii* is a nonphototrophic As(III)-oxidizing chemolithoautotroph that was isolated from the water column of Mono Lake (*14*). Analysis of its entire annotated genome revealed that it also lacks genes encoding an arsenite oxidase (e.g., *aoxAB*) but it does have two putative *arr* operons (*14*). Arsenic metabolism was not studied in *H. halophila* (*26*) although its genome contains a homolog of *arrA* (Fig. 3D) annotated as a "formate dehydrogenase." These results suggest that in the *Ectothiorhodospiraceae*, the Arr homolog is functioning in reverse or that an unknown mechanism for arsenite oxidation exists that carries out this process under anoxic conditions. Either way, it appears there are at least two distinct mechanisms for arsenite oxidation.

Over the past decade, several phylogenetically diverse microorganisms have been described that conserve energy from the oxidation or reduction of arsenic oxyanions and include deep lineages of both Bacteria and Archaea (*15*). In certain environments, a robust arsenic biogeochemical cycle supports a diverse microbial community (*25*, *27*). Our discovery of anaerobic photosynthetic oxidation of As(III) adds an important new dimension to the arsenic cycle and highlights a previously unsuspected mechanism that may have been essential for establishing and maintaining the arsenic cycle on the ancient anoxic Earth.

References and Notes

1. R. W. Castenholz, J. Bauld, B. B. Jørgensen, *FEMS Microbiol. Ecol.* **74**, 325 (1990).
2. D. J. Des Marais, *Adv. Microb. Ecol.* **14**, 251 (1995).
3. D. A. Culver, G. J. Brunskill, *Limnol. Oceanogr.* **14**, 862 (1969).
4. J. E. Cloern, B. E. Cole, R. S. Oremland, *Limnol. Oceanogr.* **28**, 1049 (1983).
5. J. J. Brocks, R. Buick, R. E. Summons, *Science* **285**, 1033 (1999).
6. R. E. Summons, L. L. Jahnke, J. M. Hope, G. A. Logan, *Nature* **400**, 554 (1999).
7. S. E. Rashby, A. L. Sessions, R. E. Summons, D. K. Newman, *Proc. Natl. Acad. Sci. U.S.A.* **104**, 15099 (2007).
8. T. Bosak, S. E. Greene, D. K. Newman, *Geobiology* **5**, 119 (2007).
9. M. M. Tice, D. R. Lowe, *Nature* **431**, 549 (2004).
10. F. Widdel, S. Schnell, S. A. Ehrenreich, B. Assmus, B. Schink, *Nature* **362**, 834 (1993).
11. A. Ehrenreich, F. Widdel, *Appl. Environ. Microbiol.* **60**, 4517 (1994).
12. B. M. Griffin, J. Schott, B. Schink, *Science* **316**, 1870 (2007).
13. J. M. Santini, L. I. Sly, R. D. Schnagl, J. M. Macy, *Appl. Environ. Microbiol.* **66**, 92 (2000).
14. S. E. Hoeft *et al.*, *Int. J. Syst. Evol. Microbiol.* **57**, 504 (2007).
15. R. S. Oremland, J. F. Stolz, *Science* **300**, 939 (2003).
16. R. S. Oremland, L.G. Miller, M. J. Whiticar, *Geochim. Cosmochim. Acta* **51**, 2915 (1987).
17. See supporting material on *Science* Online.
18. C. R. Budinoff, J. T. Hollibaugh, *ISME J.* **2**, 340 (2008).
19. Y. Cohen, E. Padan, M. Shilo, *J. Bacteriol.* **123**, 855 (1975).
20. C. R. Jackson, H. W. Langner, J. Donahoe-Christiansen, W. P. Inskeep, T. R. McDermott, *Environ. Microbiol.* **3**, 532 (2001).
21. S. D'Imperio, C. R. Lehr, M. Breary, T. R. McDermott, *Appl. Environ. Microbiol.* **73**, 7067 (2007).
22. W. P. Inskeep *et al.*, *Environ. Microbiol.* **9**, 934 (2007).
23. J. F. Stolz, P. Basu, J. M. Santini, R. S. Oremland, *Annu. Rev. Microbiol.* **60**, 107 (2006).
24. E. D. Rhine, N. Chadhain, G. J. Zylstra, L. Y. Young, *Biochem. Biophys. Res. Commun.* **354**, 662 (2007).
25. T. R. Kulp *et al.*, *Appl. Environ. Microbiol.* **72**, 6514 (2006).
26. J. C. Raymond, W. R. Sistrom, *Arch. Mikrobiol.* **69**, 121 (1969).
27. R. S. Oremland *et al.*, *Science* **308**, 1305 (2005).

28. We are grateful to the NASA Exobiology Program, the USGS, and NSF for providing research support. R. Jellison kindly made available his Mono Lake dataset to us. We thank J. Santini, D. K. Newman, J. E. Cloern, and C. Saltikov for constructive criticisms of earlier drafts of this manuscript and T. Crowe, S. Baesman, and T. Bennett for field assistance. The GenBank accession number for the arrA homolog is EU869183.

Supporting Online Material

www.sciencemag.org/cgi/content/full/321/5891/967/DC1
Methods
Figs. S1 to S3
References

21 May 2008; accepted 11 July 2008
10.1126/science.1160799

In Vivo Imaging Reveals an Essential Role for Neutrophils in Leishmaniasis Transmitted by Sand Flies

Nathan C. Peters,[1]* Jackson G. Egen,[2]*† Nagila Secundino,[1] Alain Debrabant,[3] Nicola Kimblin,[1] Shaden Kamhawi,[1] Phillip Lawyer,[1] Michael P. Fay,[4] Ronald N. Germain,[2]‡ David Sacks[1]†‡

Infection with the obligate intracellular protozoan *Leishmania* is thought to be initiated by direct parasitization of macrophages, but the early events following transmission to the skin by vector sand flies have been difficult to examine directly. Using dynamic intravital microscopy and flow cytometry, we observed a rapid and sustained neutrophilic infiltrate at localized sand fly bite sites. Invading neutrophils efficiently captured *Leishmania major* (*L.m.*) parasites early after sand fly transmission or needle inoculation, but phagocytosed *L.m.* remained viable and infected neutrophils efficiently initiated infection. Furthermore, neutrophil depletion reduced, rather than enhanced, the ability of parasites to establish productive infections. Thus, *L.m.* appears to have evolved to both evade and exploit the innate host response to sand fly bite in order to establish and promote disease.

Many parasitic diseases are transmitted by the bite of an infected arthropod, yet the dynamics of the host-parasite interaction in this context remain largely uncharacterized. Transmission of *Leishmania* by infected sand fly bite represents an attractive experimental system to study early inflammatory responses and relate these processes to the establishment of an infectious disease. Leishmaniasis is thought to be initiated by direct parasitization of macrophages after deposition into the skin (*1*). However, the ability of neutrophils to rapidly respond to and efficiently phagocytose a variety of pathogens suggests that they may also be an initial target of *Leishmania* infection (*2*–*4*). Indeed, after needle injection of *Leishmania major* (*L.m.*), infected neutrophils have been observed, and both host-protective and disease-promoting roles for these cells have been reported (*5*–*10*). How-

[1]Laboratory of Parasitic Diseases, National Institute of Allergy and Infectious Diseases, Bethesda, MD 20892, USA. [2]Laboratory of Immunology, National Institute of Allergy and Infectious Diseases, Bethesda, MD 20892, USA. [3]Laboratory of Bacterial, Parasitic, and Unconventional Agents, Division of Emerging and Transfusion Transmitted Diseases, Center for Biologics Evaluation and Research, U.S. Food and Drug Administration, Bethesda, MD 20892, USA. [4]Biostatistics Research Branch, National Institute of Allergy and Infectious Diseases, Bethesda, MD 20892, USA.

*These authors contributed equally to this work.
†To whom correspondence should be addressed. E-mail: dsacks@nih.gov (D.S.); jegen@niaid.nih.gov (J.G.E.)
‡These authors contributed equally to this work.

ever, the role of neutrophils has never been addressed in sand fly–transmitted *Leishmania* infections.

Sand fly biting involves wounding of the microvasculature to create a hemorrhagic pool from which to feed, a process that initiates a strong local inflammatory response (*11*–*13*). To further characterize the host response at the site of sand fly bite, we allowed uninfected or *L.m.*-infected *Phlebotomus duboscqi* sand flies, a natural vector of *L.m.*, to feed on the ears of C57BL/6 mice (*14*, *15*), which develop self-healing cutaneous lesions similar to the human disease. Flow cytometric analysis revealed a marked and sustained infiltration of neutrophils into the skin accompanied by a substantial recruitment of macrophages, regardless of the infectious status of the flies (Fig. 1, A and B). To visualize the bite site in vivo, we used a red fluorescent protein (RFP)–expressing strain of *L.m.* (*L.m.*-RFP) (*14*) (fig. S1, A to D) and mice expressing enhanced green fluorescent protein (eGFP) under the control of the endogenous lysozyme M promoter (LYS-eGFP mice) (*16*). $eGFP^{hi}$ cells recovered from the skin of LYS-eGFP mice after *L.m.* infection are $CD11b^{hi}Gr\text{-}1^{hi}F4/80^{-}MHCII^{-}$ neutrophils, whereas $eGFP^{lo}$ cells represent $CD11b^{+}F4/80^{+}MHCII^{+/-}Gr\text{-}1^{-}$ monocyte/macrophage populations (fig. S1, E to G; see also fig. S1, H to K). Two hours after exposure of the ventral ear pinnae of LYS-eGFP mice to either uninfected or *L.m.*-RFP–infected sand flies, $eGFP^{hi}$ neutrophils accumulated at sites of proboscis penetration through the skin (Fig. 1C).

Two-photon intravital microscopy (2P-IVM) revealed that as early as 40 min after exposure to sand flies, neutrophils had migrated into the skin and had begun to localize around apparent bite sites (Fig. 1D). Over the next hour, neutrophils rapidly accumulated in, and subsequently swarmed around, the vicinity of both infected and uninfected sand fly bites (Fig. 1D and movies S1 and S2), eventually forming an epidermal "plug" through sequential migration of neutrophils into the hole left by the sand fly proboscis (Fig. 1E, fig. S2, and movies S3 and S4). Parasite phagocytosis by neutrophils was readily observed during this recruitment process (movie S5), leading to the presence of large numbers of parasite-containing neutrophils at later time points (Fig. 1F and movie S6). In contrast to the rapid motility reported for mosquito-transmitted *Plasmodium* sporozoites, which appear to actively search for blood and lymphatic vessels (*17*, *18*), *L.m.* parasites appeared relatively immobile after sand fly delivery into the skin.

Because of the relatively low and variable number of parasites deposited by sand fly bite (*14*), we used intradermal needle inoculation of high numbers of infectious-stage *L.m.*-RFP metacyclic promastigotes to quantitatively analyze the fate of parasites post-infection (p.i.). The pattern of neutrophil recruitment at early time points was similar to sand fly bite, although comparatively short-lived (fig. S3). Two hours after injection of *L.m.*-RFP into the ear, analysis of all RFP^{+} dermal cells revealed that the vast majority of the *L.m.*-RFP signal was associated with the $CD11b^{hi}Gr\text{-}1^{hi}LYS\text{-}eGFP^{hi}$ neutrophil population (Fig. 2, A to D, and fig. S1N). These data are consistent with kinetic analyses of fixed tissue sections showing parasites initially interspersed between $F4/80^{+}eGFP^{lo}$ macrophages and subsequently phagocytosed by newly arriving $F4/80^{-}eGFP^{hi}$ neutrophils (Fig. 2, E and F).

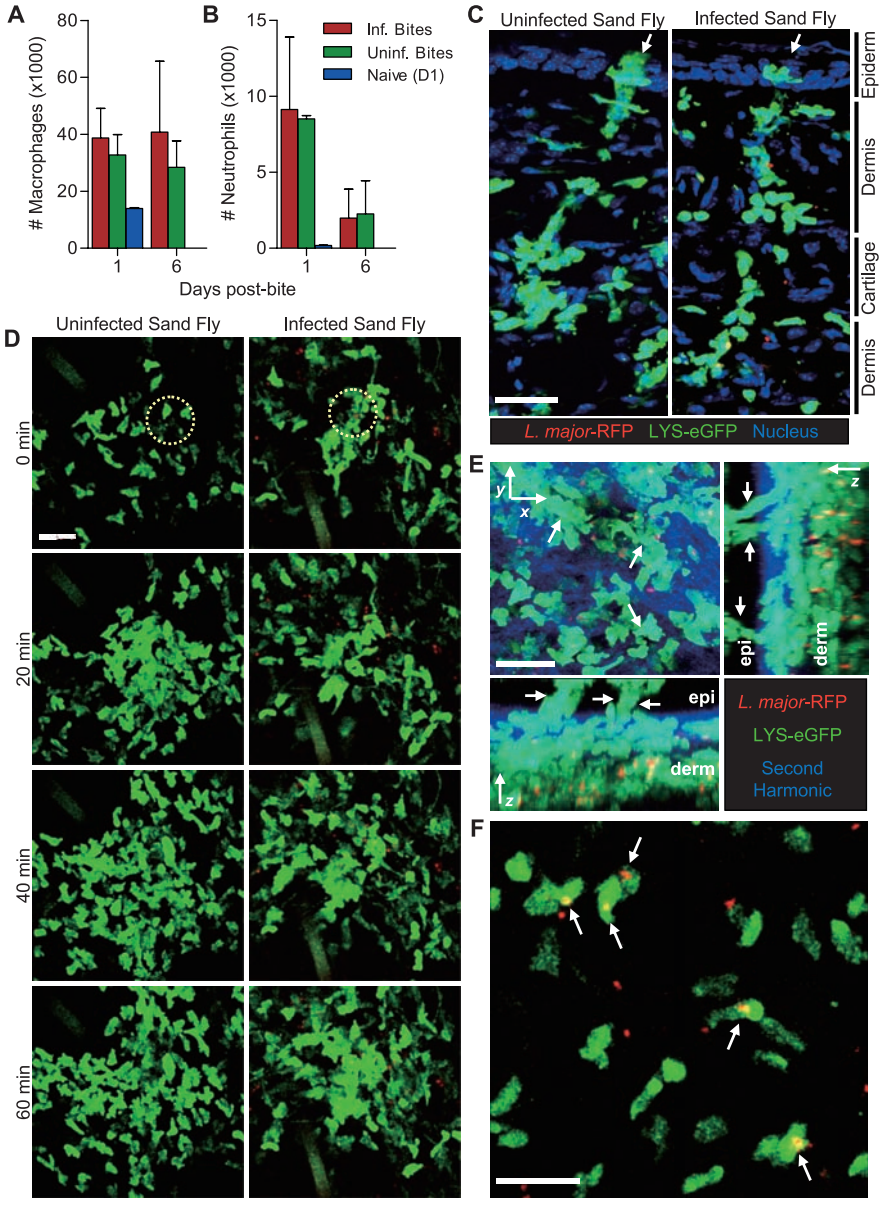

Fig. 1. Neutrophils are rapidly recruited to sites of sand fly bite, where they phagocytose *L. major* parasites. (**A** and **B**) Numbers of $CD11b^{+}F4/80^{+}$ macrophages/monocytes (A) and $CD11b^{+}Gr\text{-}1^{+}7/4^{+}F4/80^{-}MHCII^{-}Ly6G^{+}$ neutrophils (B) recruited into the ear (±SD; $n \geq 4$ ears per group per day) 1 or 6 days after being bitten by infected or uninfected sand flies. The number of cells in a naïve mouse ear is shown for day 1. (**C**) Ear sections from LYS-eGFP mice (green) bitten with uninfected sand flies (left) or *L.m.*-RFP–infected (red) sand flies (right) 2 hours before harvesting tissue. Arrows point to sites of proboscis penetration. See also movies S1 and S2. (**D**) 2P-IVM time-lapse images from the ears of LYS-eGFP mice (green) beginning 40 min after exposure to uninfected sand flies (left) or *L.m.*-RFP–infected (red) sand flies (right). Circles represent sites of sand fly proboscis penetration. (**E**) Maximum-intensity projection images across *x*, *y*, and *z* dimensions derived from 2P-IVM of the ear of a LYS-eGFP mouse (green) 2 hours after exposure to *L.m.*-RFP–infected (red) sand flies. Dermal and epidermal layers defined by the presence or absence of collagen (blue), respectively, are indicated. Arrows point to sites of proboscis penetration and neutrophil "plug" formation. See also movies S3 and S4. (**F**) Image obtained from a 2P-IVM time-lapse series of the ear of a LYS-eGFP mouse (green) 3 hours after exposure to *L.m.*-RFP–infected (red) sand flies. Arrows point to neutrophils with one or more intracellular parasites. See also movies S5 and S6. Scale bars, 30 μm [(C) to (E)], 20 μm (F).

Dynamic analysis of neutrophil recruitment and parasite uptake revealed the rapid accumulation of neutrophils inside blood vessels surrounding the infection site as early as 30 min p.i. and the subsequent diapedesis of these cells into the skin parenchyma (Fig. 2G and movie S7). Extravasating neutrophils were preferentially distributed to the side of the vessel facing parasite deposition and were characterized by an extremely elongated uropod (Fig. 2H and movie S8). Neutrophils then moved in a highly directed manner toward the inoculation site (Fig. 2, G to I), where they rapidly and efficiently phagocytosed individual parasites (Fig. 2J). Phagocytosis occurred concurrently with migrational arrest, as revealed by a decrease in neutrophil mean velocity after parasite uptake (Fig. 2K). Additional data acquired after needle inoculation in the absence of parasites suggest that the initial inflammatory response to sand fly bite or needle-induced tissue damage drives the robust neutrophilic recruitment observed in these studies, overriding the potential contribution of any parasite-specific signals (fig. S4 and movie S9).

Because macrophages are the definitive host cell for *Leishmania*, we explored their relationship with neutrophils. Mice expressing eGFP under the control of the endogenous major histocompatibility complex class II promoter (MHCII-eGFP) (*19*) (fig. S1, L and M) were inoculated with *L.m.*-RFP. Phenotypic analysis of RFP-gated dermal cells at 18 hours p.i. revealed that the RFP signal was primarily associated with CD11b^{hi}Gr-1^{hi}MHC-II-eGFP^{-} neutrophils and only small numbers of monocytes/macrophages or CD11c^{+} dendritic cells (DCs) (Fig. 3A and fig. S5). Strikingly, we observed an increase in the absolute number of RFP^{+} macrophages and a corresponding drop in the absolute number of RFP^{+} neutrophils over time (Fig. 3, C and D). By 6 to 7 days p.i., the RFP signal was found primarily in the macrophage/monocyte population and only sparsely in neutrophils and CD11c^{+} DCs (Fig. 3, B, D, and E). Although MHC-II-eGFP^{+}CD11c^{+} cells represented an extremely small proportion of infected cells at 1 day p.i., their increase in numbers by day 6 suggests that dermal DCs and/or Langerhans cells participate in the infectious process (*20*).

To determine the fate of *Leishmania* promastigotes after phagocytosis by neutrophils in vivo, we isolated infected and uninfected neutrophils from the ear dermis by cell sorting (Fig. 4, A to C). eGFP^{hi}RFP^{+} cells retained a normal cytoplasmic and nuclear appearance and contained intracellular *L.m.* parasites (Fig. 4D) (*21*). Limiting dilution analysis of sorted neutrophils revealed that 92% of RFP^{+} but only 1.2% of RFP^{-} neutrophils contained at least one viable parasite (Fig. 4E). Furthermore, naïve mice inoculated with 10^{3} RFP^{+}GFP^{+} neutrophils or 10^{3} cultured *L.m.*-RFP established equivalent infections (Fig. 4, F to H), which demonstrates that *L.m.* phagocytosed by neutrophils are viable and can contribute to the establishment and progression of disease.

The extremely dense clusters of eGFP-expressing neutrophils and macrophages/monocytes that formed several hours after parasite inoculation (Fig. 3E) made visualization of individual cell-cell interactions difficult. To overcome this problem, we injected sorted eGFP^{hi}RFP^{+} infected neutrophils into the ears of transgenic animals expressing eGFP under the control of the macrophage/monocyte-specific CSF1 receptor promoter (*22*). Recipient animals were preexposed to sand flies 12 hours before neutrophil transfer to induce an inflammatory environment at the infection site.

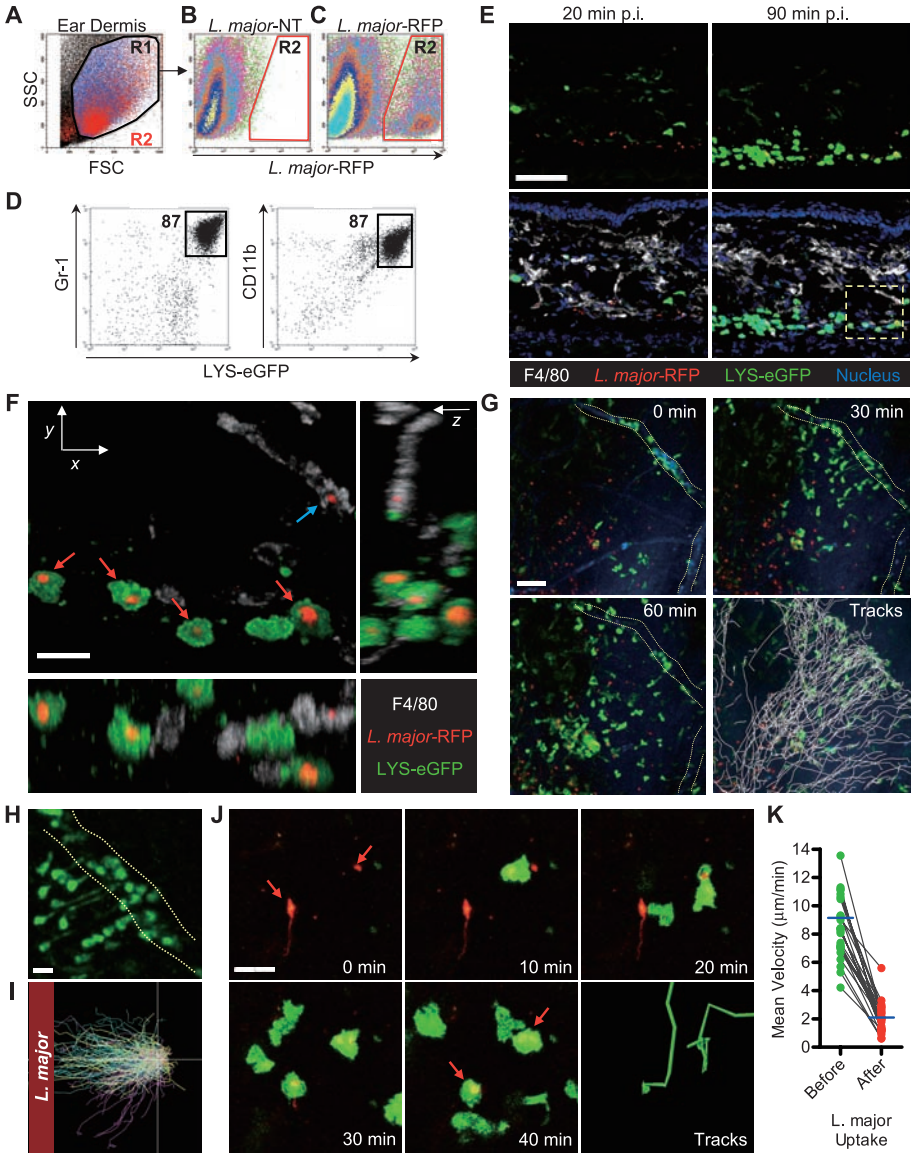

Fig. 2. Rapid recruitment and infection of neutrophils after intradermal inoculation of *L. major*. (**A**) Side scatter (SSC)/forward scatter (FSC) dot plot of ear-derived cells 16 hours p.i. with 10^{6} *L.m.*-RFP. (**B** and **C**) SSC/RFP dot plots of R1-gated ear cells 16 hours p.i. with 10^{6} *L.m.*—empty vector control (B) or *L.m.*-RFP (C). (**D**) GFP, Gr-1, and CD11b expression by RFP^{+} R2-gated cells from ears of LYS-eGFP mice 2 hours p.i. with 5 × 10^{5} *L.m.*-RFP. (**E**) Ear sections from LYS-eGFP mice 20 min (left) or 90 min (right) p.i. with 10^{4} *L.m.*-RFP stained with F4/80 (white) and a nuclear dye (blue). Top panels show GFP and RFP images; bottom panels show a merge of all channels. (**F**) Maximum-intensity projection images across *x*, *y*, and *z* dimensions from boxed region in (E). Red arrows indicate *L.m.*-RFP phagocytosed by neutrophils; blue arrow indicates a parasite captured by a macrophage. (**G** to **K**) LYS-eGFP animals were subjected to 2P-IVM 30 min p.i. with 10^{4} *L.m.*-RFP. (G) Time-lapse images showing GFP^{+} (green) cells, *L.m.*-RFP (red), and blood vessels (blue). Panel labeled "Tracks" shows the paths followed by cells from the vessel to site of inoculation of parasites over 60 min. (H) Magnified view from (G) showing neutrophil extravasation from vasculature. See also movies S7 and S8. (I) Cell migration paths from three independent experiments (cyan, yellow, and purple tracks) were normalized for their origin and their position relative to the site of parasite deposition. (J) Time-lapse images showing neutrophil (green) migration before and after phagocytosis of *L.m.*-RFP (red, arrows). (K) Neutrophil mean velocity 10 min before and 10 min after parasite phagocytosis. Data points represent individual cells and were compiled from four separate experiments. Scale bars, 50 μm [(E) and (G)], 15 μm [(F), (H), and (J)].

Using 2P-IVM, we observed what appeared to be viable parasites [as indicated by their expression of RFP (fig. S1, A to D)] being released from apoptotic neutrophils in the vicinity of surrounding macrophages (fig. S6 and movies S10 to S12).

We next examined the functional role of neutrophils on the establishment and progression of sand fly–transmitted leishmaniasis. Mice treated

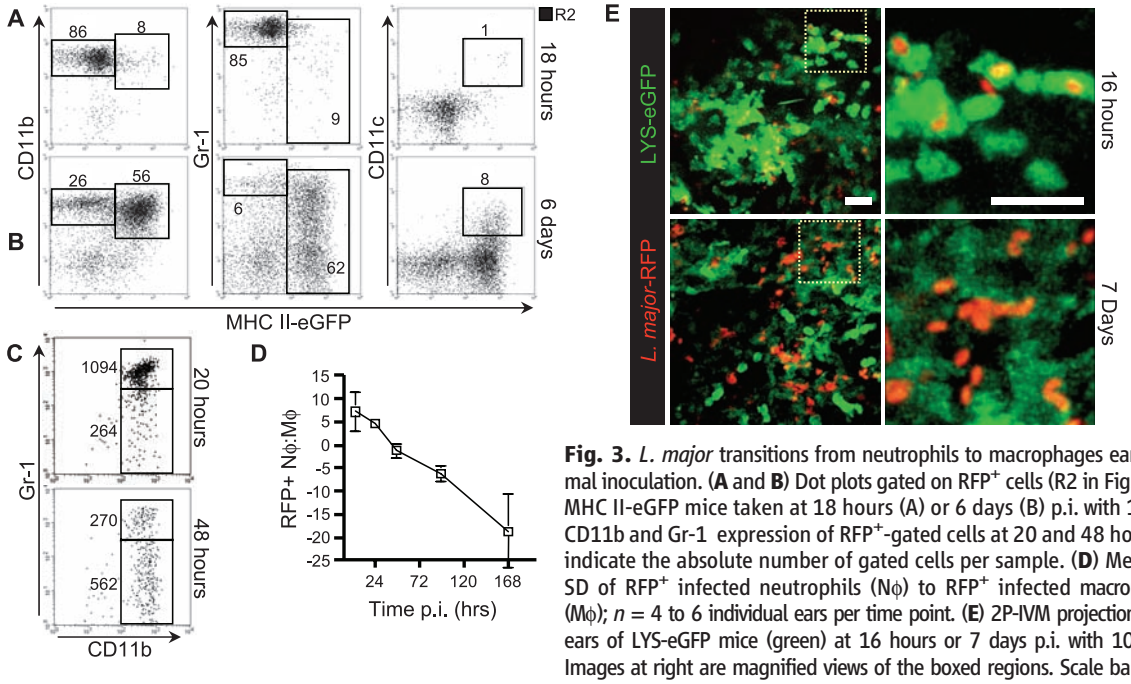

Fig. 3. *L. major* transitions from neutrophils to macrophages early after intradermal inoculation. (**A** and **B**) Dot plots gated on RFP$^+$ cells (R2 in Fig. 2C) from ears of MHC II-eGFP mice taken at 18 hours (A) or 6 days (B) p.i. with 10^6 *L.m.*-RFP. (**C**) CD11b and Gr-1 expression of RFP$^+$-gated cells at 20 and 48 hours p.i. Numbers indicate the absolute number of gated cells per sample. (**D**) Mean of the ratio ± SD of RFP$^+$ infected neutrophils (Nϕ) to RFP$^+$ infected macrophages/monocytes (Mϕ); $n = 4$ to 6 individual ears per time point. (**E**) 2P-IVM projection images from the ears of LYS-eGFP mice (green) at 16 hours or 7 days p.i. with 10^4 *L.m.*-RFP (red). Images at right are magnified views of the boxed regions. Scale bars, 20 μm.

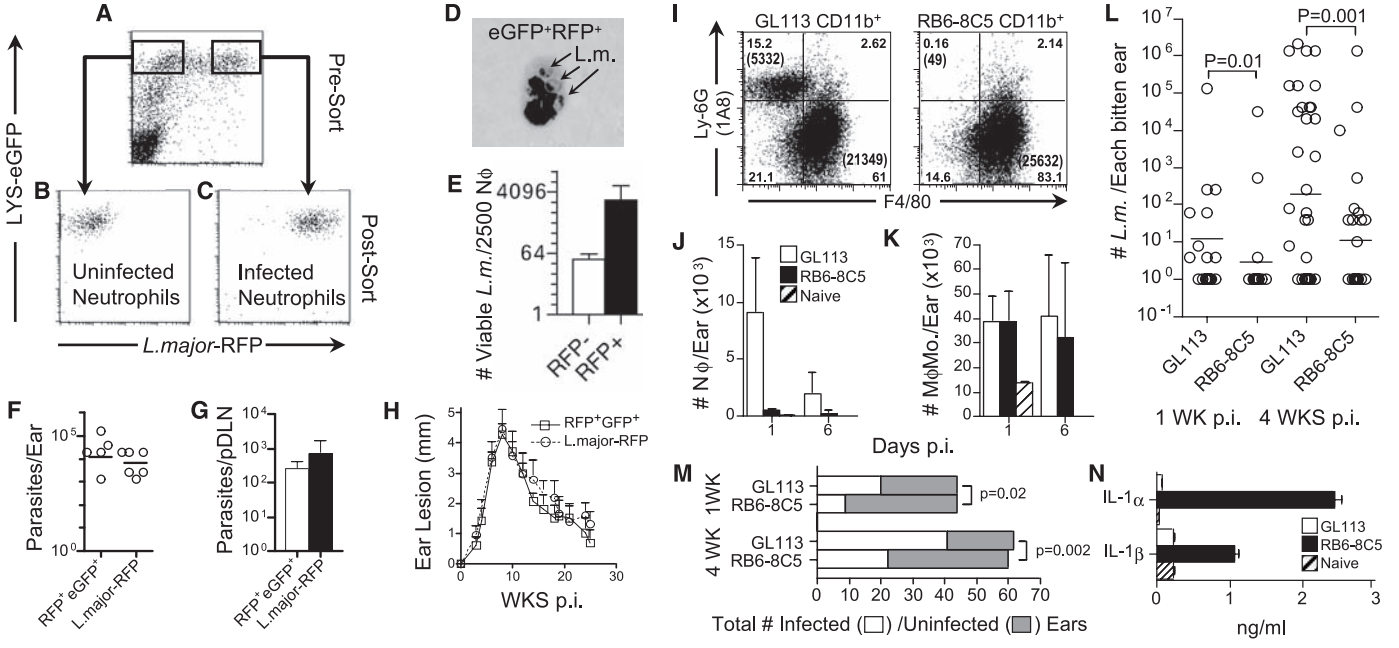

Fig. 4. Neutrophils harbor viable parasites and promote productive infections. (**A** to **D**) LYS-eGFP^{hi} neutrophils from the ear 12 hours p.i. with 2.5×10^6 *L.m.*-RFP were sorted into uninfected RFP$^-$ (B) or *L.m.*-infected RFP$^+$ [(C) and (D)] populations. [(B) and (C)] Post-sort. (D) Dif-Quick stain of the cytospun eGFP$^+$RFP$^+$ post-sort population. (**E**) Number of viable parasites per 2500 RFP$^-$ and RFP$^+$ neutrophils (±SD of triplicate samples). (**F** to **H**) Wild-type mice were injected in the ear with 10^3 culture-derived *L.m.*-RFP metacyclic promastigotes or 10^3 RFP$^+$eGFP^{hi} infected neutrophils. Twenty-one days after injection, mice were assessed for parasite load in individual ears (F), pooled draining lymph nodes (pDLNs) (G), and mean ± SEM ($n = 8$) ear lesion diameter over the course of infection (H). (**I** to **N**) Mice were treated with control (GL113) or neutrophil-depleting (RB6-8C5) monoclonal antibodies 16 hours before exposure to infected sand flies. (I) Representative dot plot of CD11b$^+$-gated Ly-6G$^+$F4/80$^-$ neutrophils and Ly6G$^-$F4/80$^+$ macrophages/monocytes on day 1 p.i. [(J) and (K)] Analysis of the total number of CD11b$^+$7/4$^+$F4/80$^-$MHCII$^-$Ly6G$^+$ neutrophils (J) and CD11b$^+$F4/80$^+$ macrophage/monocytes (K), per ear ± SD ($n \geq 4$ per group per day), on day 1 and day 6 p.i. (L) Parasite loads in individual ears at 1 and 4 weeks after exposure to infected sand flies in GL113-treated versus RB6-8C5–treated animals, as determined by limiting dilution analysis. Each open circle represents a single exposed ear in three (1 week) or four (4 weeks) pooled experiments. (M) Representation of the total incidence of infected versus uninfected ears in RB6-8C5– versus GL113-treated animals at 1 week [odds ratio = 0.299, 95% CI (0.097, 0.847), $P = 0.020$] and 4 weeks [odds ratio = 0.293, 95% CI (0.126, 0.658), $P = 0.0017$] after transmission, as determined by limiting dilution analysis. (N) Spontaneous release of interleukin-1α and 1β by ear derived cells, as determined by multiplex cytokine analysis at 1 week p.i.

with neutrophil-depleting antibody 16 hours before infected sand fly exposure had a specific and marked reduction of $CD11b^+Ly\text{-}6G^+F4/80^-$ neutrophils in the ear dermis 1 day after transmission (Fig. 4, I and J), whereas the $CD11b^+Ly\text{-}6G^-F4/80^+$ macrophage/monocyte population was unaffected (Fig. 4, I and K). In some but not all experiments, reduced numbers of neutrophils were also observed in ears 6 days after transmission (Fig. 4J). Neutrophil depletion significantly reduced the number of viable parasites detected per ear (Fig. 4L), as well as the incidence of ears with detectable parasites at 1 and 4 weeks after transmission (Fig. 4M). Thus, the early influx and persistence of neutrophils after sand fly transmission of *L.m.* appears critical for the development of cutaneous disease.

The data presented here are relevant to the "Trojan horse" model of *L.m.* infection (*2*), which postulates that uptake of infected neutrophils is a mechanism for "silent" entry of parasites into macrophages. Our observations indicate that neutrophils are the initial host cell for a substantial fraction of parasites after infection and that neutrophil depletion results in reduced disease at 1 week p.i. We found no evidence, however, for uptake of intact, infected neutrophils by macrophages. In addition, macrophages were efficiently recruited to sites of infection and were able to directly phagocytose parasites in neutrophil-depleted animals (fig. S7). Under these conditions, macrophages and DCs did not acquire more parasites relative to nondepleted animals containing competing neutrophils, which suggests that neutrophils may facilitate infection by rescuing parasites not accessible to other phagocytic cells from death in extracellular spaces. Alternatively, infected neutrophils may release transitional-stage parasites better adapted for macrophage uptake and survival, or macrophages may exhibit compromised microbicidal function in a setting in which they are heavily engaged in the anti-inflammatory process of clearing apoptotic neutrophils (*23*, *24*). This latter possibility is supported by an increase in the spontaneous release of the proinflammatory cytokines interleukin-1α and 1β by ear cells from neutrophil-depleted animals (Fig. 4N) (*25*).

The ability of phagocytic cells to rapidly localize to sites of tissue inflammation and subsequently capture and destroy pathogens is a hallmark of the innate immune response, highly conserved, and among the earliest observations in microbiology (*26*). We found that sand fly bites and needle inoculation induce an intense neutrophilic infiltrate into the skin, irrespective of parasite infection. These data are consistent with the finding that neutrophils are recruited to sites of sterile brain injury (*27*) and suggest that the predominance of *L.m.*-infected neutrophils at the site of parasite deposition is a by-product of a host response aimed at wound repair and sterilization. Thus, the neutrophilic host response to the wound inflicted by arthropod vectors appears to have been a driving force in pathogen evolution aimed at counteracting and even exploiting the presence of these innate effector cells.

References and Notes

1. N. Peters, D. Sacks, *Immunol. Rev.* **213**, 159 (2006).
2. G. van Zandbergen, W. Solbach, T. Laskay, *Autoimmunity* **40**, 349 (2007).
3. A. W. Segal, *Annu. Rev. Immunol.* **23**, 197 (2005).
4. W. M. Nauseef, *Immunol. Rev.* **219**, 88 (2007).
5. Y. Belkaid *et al.*, *J. Immunol.* **165**, 969 (2000).
6. F. L. Ribeiro-Gomes, M. T. Silva, G. A. Dosreis, *Parasitology* **132** (suppl.), S61 (2006).
7. M. Charmoy *et al.*, *J. Leukoc. Biol.* **82**, 288 (2007).
8. F. Tacchini-Cottier *et al.*, *J. Immunol.* **165**, 2628 (2000).
9. L. Chen *et al.*, *Parasitol. Int.* **54**, 109 (2005).
10. G. van Zandbergen *et al.*, *J. Immunol.* **173**, 6521 (2004).
11. C. R. Teixeira *et al.*, *J. Immunol.* **175**, 8346 (2005).
12. S. Kamhawi, Y. Belkaid, G. Modi, E. Rowton, D. Sacks, *Science* **290**, 1351 (2000).
13. Y. Belkaid *et al.*, *Proc. Natl. Acad. Sci. U.S.A.* **97**, 6704 (2000).
14. N. Kimblin *et al.*, *Proc. Natl. Acad. Sci. U.S.A.* **105**, 10125 (2008).
15. See supporting material on *Science* Online.
16. N. Faust, F. Varas, L. M. Kelly, S. Heck, T. Graf, *Blood* **96**, 719 (2000).
17. R. Amino *et al.*, *Nat. Med.* **12**, 220 (2006).
18. J. P. Vanderberg, U. Frevert, *Int. J. Parasitol.* **34**, 991 (2004).
19. M. Boes *et al.*, *Nature* **418**, 983 (2002).
20. L. Soong, *J. Immunol.* **180**, 4355 (2008).
21. E. Aga *et al.*, *J. Immunol.* **169**, 898 (2002).
22. S. H. Burnett *et al.*, *J. Leukoc. Biol.* **75**, 612 (2004).
23. D. V. Krysko, K. D'Herde, P. Vandenabeele, *Apoptosis* **11**, 1709 (2006).
24. C. D. Gregory, A. Devitt, *Immunology* **113**, 1 (2004).
25. C. Matte, M. Olivier, *J. Infect. Dis.* **185**, 673 (2002).
26. P. Martin, S. J. Leibovich, *Trends Cell Biol.* **15**, 599 (2005).
27. J. V. Kim, M. L. Dustin, *J. Immunol.* **177**, 5269 (2006).

28. We thank K. Beacht for technical assistance; H. Qi, M. Bajénoff, S. Nylén, and M. A. McDowell for discussions; T. Moyer and C. Henry for neutrophil sorting; and A. Rothfuchs for GL113 and RB6-8C5 monoclonal antibodies. Supported by the Intramural Research Program of the NIAID.

Supporting Online Material

www.sciencemag.org/cgi/content/full/321/5891/970/DC1
Materials and Methods
Figs. S1 to S7
Movies S1 to S12
References

16 April 2008; accepted 4 July 2008
10.1126/science.1159194

Tumor Regression in Cancer Patients by Very Low Doses of a T Cell–Engaging Antibody

Ralf Bargou,[1,2]* Eugen Leo,[3]*† Gerhard Zugmaier,[3] Matthias Klinger,[3] Mariele Goebeler,[1,2] Stefan Knop,[2] Richard Noppeney,[4] Andreas Viardot,[5] Georg Hess,[6] Martin Schuler,[7] Hermann Einsele,[2] Christian Brandl,[3] Andreas Wolf,[3] Petra Kirchinger,[3] Petra Klappers,[3] Margit Schmidt,[3] Gert Riethmüller,[8] Carsten Reinhardt,[3] Patrick A. Baeuerle,[3]‡ Peter Kufer[3]

Previous attempts have shown the potential of T cells in immunotherapy of cancer. Here, we report on the clinical activity of a bispecific antibody construct called blinatumomab, which has the potential to engage all cytotoxic T cells in patients for lysis of cancer cells. Doses as low as 0.005 milligrams per square meter per day in non–Hodgkin's lymphoma patients led to an elimination of target cells in blood. Partial and complete tumor regressions were first observed at a dose level of 0.015 milligrams, and all seven patients treated at a dose level of 0.06 milligrams experienced a tumor regression. Blinatumomab also led to clearance of tumor cells from bone marrow and liver. T cell–engaging antibodies appear to have therapeutic potential for the treatment of malignant diseases.

Substantial evidence suggests that cytotoxic T lymphocytes participate in controlling tumor growth and that they can be harnessed in immunotherapeutic settings. For example, their presence in colorectal tumors was shown to strongly predict clinical outcome (*1*), and adoptive transfer of ex vivo expanded tumor-derived lymphocytes (*2*) or of T cell receptor gene transfected T cells to melanoma patients (*3*) has been shown to lead to cancer regression. However, therapies aimed at inducing specific T cell responses against cancer cells, including vaccination (*4*) and CTLA-4–blocking antibodies (*5*), have been limited by relatively low response rates and relapses, presumably because of immune escape mechanisms of cancer cells (*6*, *7*).

An alternative approach to harness the high cytotoxic potential of T cells has been the use of T cell–engaging antibodies (*8*, *9*). Conventional antibodies are not able to directly recruit T cells because these cells lack Fcγ receptors. Well-studied antibody constructs for engaging T cells are bispecific T cell engagers (BiTE), which are based on single-chain antibodies (*10*, *11*). These molecules can transiently tether resting T cells to tumor cells, leading to concomitant T cell activation and serial lysis of tumor cells (*12*–*14*). To date, various mouse models have demonstrated high levels of activity of BiTE antibodies (*15*–*20*). The independence of this approach from peptide antigen presentation and tumor-specific T cell clones suggests that it can overcome major immune escape mechanisms.

We have investigated clinical activity and safety of increasing doses of BiTE antibody blinatumomab (also called MT103/MEDI-538) with dual specificity for CD19 and CD3 (*21*–*24*)